nature materials

ARTICLES

PUBLISHED ONLINE: 18 OCTOBER 2009 | DOI: 10.1038/NMAT2565

Small-molecule-directed nanoparticle assembly towards stimuli-responsive nanocomposites

Yue Zhao[1]*, Kari Thorkelsson[1]*, Alexander J. Mastroianni[1,2,3]*, Thomas Schilling[1], Joseph M. Luther[2,3], Benjamin J. Rancatore[1,2,3], Kazuyuki Matsunaga[4], Hiroshi Jinnai[4,5], Yue Wu[2], Daniel Poulsen[2], Jean M. J. Fréchet[2,3], A. Paul Alivisatos[2,3] and Ting Xu[1,2,3]†

Precise control of the spatial organization of nanoscopic building blocks, such as nanoparticles, over multiple length scales is a bottleneck in the 'bottom-up' generation of technologically important materials. Only a few approaches have been shown to achieve nanoparticle assemblies without surface modification. We demonstrate a simple yet versatile approach to produce stimuli-responsive hierarchical assemblies of readily available nanoparticles by combining small molecules and block copolymers. Organization of nanoparticles into one-, two- and three-dimensional arrays with controlled inter-particle separation and ordering is achieved without chemical modification of either the nanoparticles or block copolymers. Nanocomposites responsive to heat and light are demonstrated, where the spatial distribution of the nanoparticles can be varied by exposure to heat or light or changing the local environment. The approach described is applicable to a wide range of nanoparticles and compatible with existing fabrication processes, thereby enabling a non-disruptive approach for the generation of functional devices.

Facile control over the spatial distribution of nanoscopic building blocks, such as nanoparticles, from nanoscopic to macroscopic length scales, has been a major impediment in the 'bottom-up' fabrication of functional materials. Precise manipulation of nanoparticle assemblies would enable one to capitalize on the plethora of available nanoparticles with unique optical, electronic or magnetic properties so as to generate functional devices, ranging from sensors and memory storage to photovoltaic, plasmonic and other microelectronic devices[1–5]. Albeit challenging, further control using external stimuli to direct the ordering and local environment of nanoparticles would be ideal for the design of responsive functional nanocomposites[6,7].

Various routes to direct nanoparticle assemblies have been explored, including the use of DNA and functional polymers[1,2,8–14]. Programmable DNA linkers have been shown to be effective in obtaining nanoparticle arrays with tunable symmetry and dimensionality. However, large-scale fabrication poses a significant hurdle for many practical applications[1]. Block copolymers (BCPs), on the other hand, self-assemble into well-defined arrays of nanostructures over macroscopic distances, presenting an ideal platform for directing the assembly of nanoparticles[11,12,15–17]. However, directing the nanoparticle assembly within BCP microdomains that are tens of nanometres in size and obtaining external-stimuli-responsive nanocomposites still remains a challenge. BCP chains assume a stretched, random coil configuration and provide less control over the nanoparticle assembly, generally leading to a random distribution of nanoparticles within the microdomains. Incorporating stimuli-responsiveness into a BCP without interfering with the nanoparticle assemblies can be synthetically challenging, making it non-trivial to generate responsive nanocomposites. Furthermore, using only BCPs to guide nanoparticle assemblies requires a delicate balance between the interactions of the nanoparticle ligands and the segments of the BCPs and the entropic penalties arising from the perturbation of the BCP chain configuration[10,11,13,18–26]. Modifying the ligands of the nanoparticles to make them compatible with a specific BCP is possible, but usually requires synthetic procedures that are specific to each nanoparticle core and can be synthetically challenging[22,27–29]. Perturbing the ligand shell in exchange reactions can also alter the properties of the nanoparticles[30].

Small molecules, in comparison to BCPs, are more easily synthesized so as to design in specific functionality or intermolecular interactions. By attaching small molecules that favourably interact with the nanoparticle ligands to the polymer side chains in a non-covalent manner, for example by hydrogen bonding or electrostatic interactions, nanoparticle–polymer interactions can be tailored[31–36]. This decouples the nanoparticle surface chemistry and the chemical constitution of the BCP, eliminates the need to modify either the nanoparticle ligands or the polymer and thus significantly expands the repertoire of nanoparticles that can be solubilized in polymers. The non-covalent linkage between the small molecules and BCP can be strengthened or broken by external stimuli[35,37–39], resulting in changes of the chain configuration, a redistribution of the small molecules and, therefore, a change in the spatial distribution of the nanoparticles. Functional, stimuli-responsive small molecules can be readily substituted to fine-tune or incorporate specific properties. Therefore, the local environment and spatial arrangement of the nanoparticles can be tailored, opening further routes to manipulate the properties of these nanocomposites. The attachment of small molecules to one block of the BCP changes the architecture of the BCP from a coil–coil to a coil–comb BCP and, also, the configuration of the BCP backbone chain, providing a unique handle to direct nanoparticle assembly at a single polymer

[1]Department of Materials Science and Engineering, University of California, Berkeley, California 94720-1760, USA, [2]Department of Chemistry, University of California, Berkeley, California 94720-1760, USA, [3]Material Sciences Division, Lawrence Berkeley National Laboratory, Berkeley, California 94720, USA, [4]Kyoto Institute of Technology, Kyoto 606-8585, Japan, [5]WPI Advanced Institute for Materials Research, Tohoku University, Sendai 980-8577, Japan. *These authors contributed equally to this work. †e-mail: tingxu@berkeley.edu.

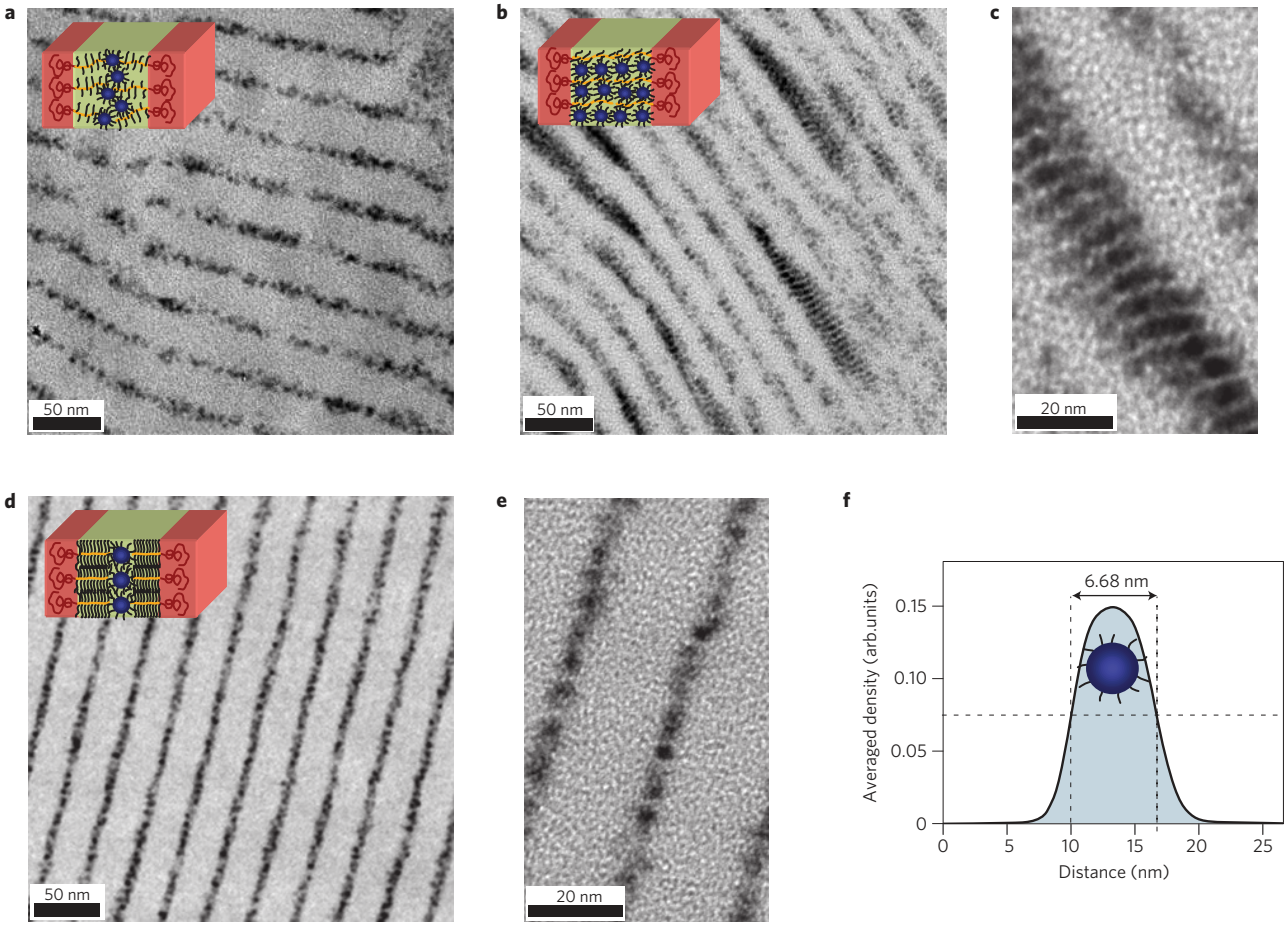

Figure 1 | TEM images of blends of PS(40)-*b*-P4VP(5.6)(PDP)$_r$ and various nanoparticles. a, A blend of PS(40)-*b*-P4VP(5.6)(PDP)$_1$ and ~4 nm CdSe (~2 vol%) nanoparticles, where the CdSe nanoparticles are selectively incorporated into the lamellar P4VP(PDP)$_1$ microdomains. **b**,**c**, A blend of PS(40)-*b*-P4VP(5.6)(PDP)$_1$ and ~5.4 nm PbS (~7 vol%) nanoparticles. PbS nanoparticles are assembled in the centre of the P4VP(PDP)$_1$ lamellae or into layers oriented normal to the lamellar interfaces. Schematic drawings of both nanoparticle assemblies are also shown. **d**,**e**, A blend of PS(40)-*b*-P4VP(5.6)(PDP)$_2$ and ~4 nm CdSe (~2 vol%) nanoparticles. **f**, Image analysis on the nanoparticle spatial distribution within the BCP lamellae. The full-width at half-maximum is 6.68 nm for 4 nm nanoparticles and the deviation of the nanoparticle distribution is only 67% of the CdSe nanoparticle size.

chain level. The change in the entropy of the BCP chain arising from the incorporation of the nanoparticles depends on the polymer chain architecture and its stiffness[40]. These provide further controls for tailoring the thermodynamics of the assembly process[19,20]. In addition, the small molecules constituting the teeth of the comb-block can order on the molecular level within the BCP microdomains[36], resulting in hierarchical assemblies that can further guide the spatial distribution of the nanoparticles with a precision akin to that seen when using DNA, but over large lateral areas.

Here, two small molecules, 3-*n*-pentadecylphenol (PDP) and 4-(4′-octylphenyl)azophenol (OPAP), that hydrogen bond to a BCP, polystyrene-*block*-poly(4-vinyl pyridine) (PS-*b*-P4VP) were used to precisely direct nanoparticle assemblies over multiple length scales. We demonstrate that thermo- and light-responsive, hierarchical assemblies of a wide range of nanoparticles, independent of size and shape, can be produced without chemically modifying the nanoparticles or BCPs. The approach described can be extended to small molecules with built-in functionalities and stimuli-responsiveness. This directed co-assembly of small molecules, BCPs and nanoparticles overcomes many impediments in 'bottom-up' fabrication and opens new routes to precisely control the spatial distribution of nanoscale materials over multiple length scales and to generate stimuli-responsive nanocomposites.

A PS-*b*-P4VP BCP with polystyrene and P4VP with block molecular weights of 40 and 5.6 kDa, was used. The phenol group of PDP hydrogen bonds to the 4VP units of the P4VP and, as shown previously, forms a PS-*b*-P4VP(PDP)$_r$ (the subscript r denotes the ratio of PDP to 4VP units) supramolecule[41]. PS(40)-*b*-P4VP(5.6)(PDP)$_1$ forms a lamellae-within-lamellae hierarchical assembly[41]. PDP was used, as the alkyl tail is similar to the alkane ligands used to stabilize many nanoparticles. Other small molecules that can interact with the BCP and the nanoparticle ligands could also have been used. In a blend of PS(40)-*b*-P4VP(5.6)(PDP)$_1$, $r = 1$, with 4 nm CdSe nanoparticles (~2 vol%) capped with octadecylphosphonate ligands, the transmission electron microscopy (TEM) and small angle X-ray scattering (SAXS) (see Supplementary Fig. S3) studies showed that without surface modification, the CdSe nanoparticles were exclusively incorporated into the P4VP(PDP)$_r$ lamellar microdomains as shown in Fig. 1a. The comb-block, P4VP(PDP)$_r$, assembles within the BCP microdomains and can further direct the nanoparticle assembly increasing the volume fraction of nanoparticles to 7% (5.4 nm PbS nanoparticles capped with oleate ligands are used in this case), two different types of ordering are observed (Fig. 1b,c). In addition to the sequestration of the PbS nanoparticles in the centre of the P4VP(PDP)$_1$ microdomains, the PbS nanoparticles also are seen to intercalate between the P4VP(PDP)$_1$ comb-blocks within the BCP lamellae.

Directing the nanoparticle localization on blending with BCP requires specific nanoparticle–polymer interactions. This was

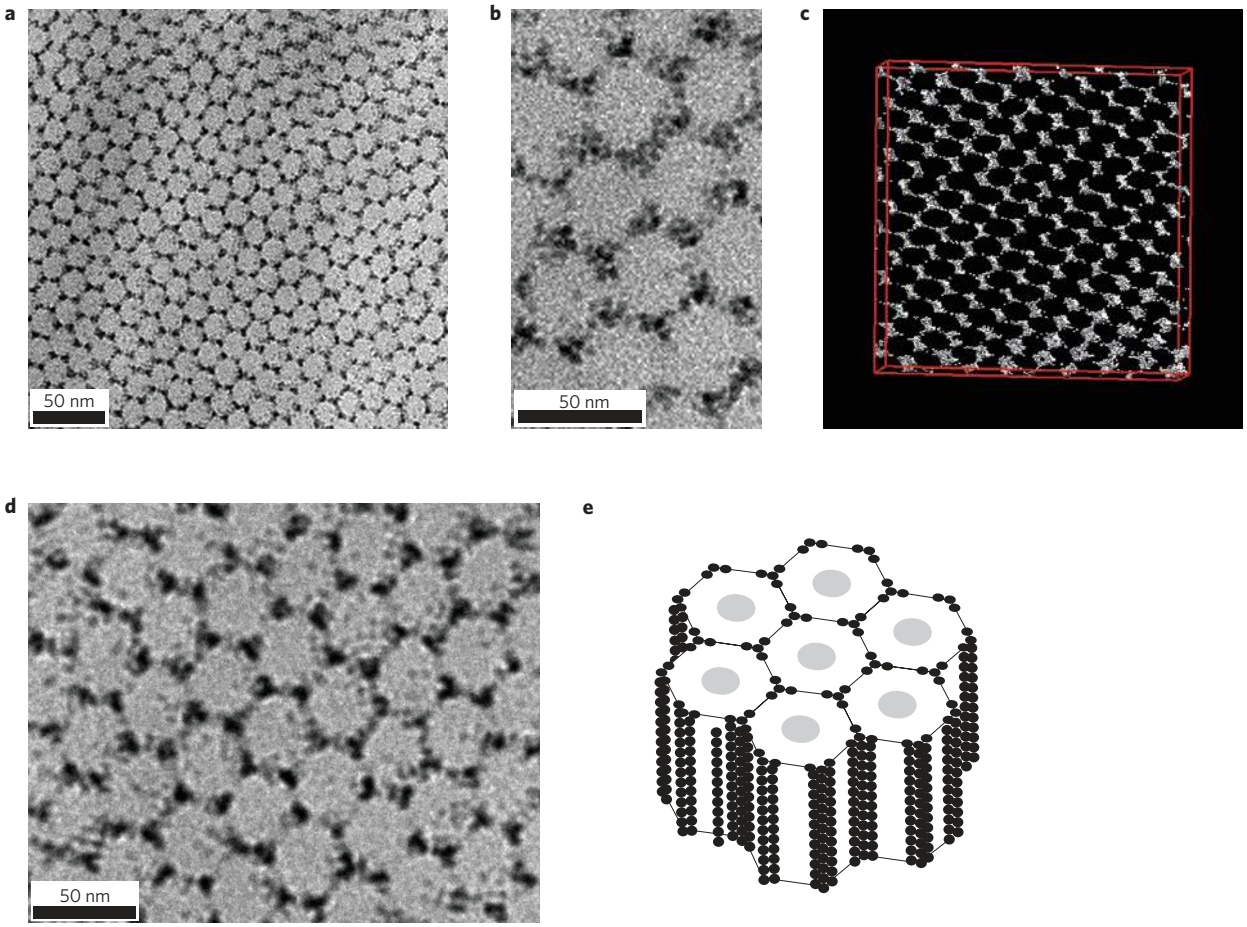

Figure 2 | A blend of PS(40)-*b*-P4VP(5.6)(PDP)$_3$ and ~5.4 nm PbS (~7 vol%) nanoparticles, showing the PbS nanoparticles arranged in a hexagonal grid. a,**b**, TEM images. **c**, TEM tomography image. **d**, TEM image of the same blend in the region with lower PbS nanoparticle loadings. **e**, Schematic diagram showing that the PbS nanoparticles are preferentially sequestered in the corners of the hexagons.

previously achieved by either nanoparticle ligand exchange or modification[11,12,22]. However, changing the nanoparticle ligand shell can alter the properties of the nanoparticles and for many nanoparticles, be synthetically challenging. To capitalize on the inherent characteristics of the nanoparticles, it is essential to modify the nanoparticle surfaces in a non-perturbing manner and best of all, to use the native ligands on the nanoparticles remaining from their synthesis. In our case, nanoparticle ligand modification is unnecessary because the favourable interactions between the PDP and the nanoparticle's native alkyl ligands selectively incorporate the nanoparticles into the P4VP(PDP)$_r$ microdomain, independent of the nanoparticle shape and size. Similar results were found with a large variety of nanoparticles with different sizes and shapes, including $CoFe_2O_4$ dots (6 nm), Au dots (3–20 nm), PbS dots (2 nm), CdSe dots (2 nm) and CdSe nanorods (3 nm × 20 nm and 6 nm × 17 nm) (see Supplementary Fig. S4). In all cases, it was not necessary to modify either the BCPs or nanoparticles. The entropy associated with the polymer chain deformation on incorporating the nanoparticles also has an important part in the nanoparticle spatial distribution[16,17,19]. In our approach, no size dependence on the spatial distribution of the nanoparticles in the nanoparticle/supramolecule blends was observed. The TEM image in Supplementary Fig. S4.1 shows that Au nanoparticles of different sizes—where the ratio of the nanoparticle size (d) and the equilibrium period of the supramolecule/nanoparticle blend (L), d/L, ranged from 0.075 to 0.4—assembled at the centre of the P4VP(PDP)$_1$ lamellae.

Dispersing nanoparticles within the BCP microdomain alters the BCP chain configuration, where the entropic penalty depends on the polymer chain stiffness, architecture and nanoparticle size. By attaching PDP to 4VP, P4VP changes from a random coil to a P4VP(PDP)$_r$ comb that orders within the P4VP(PDP)$_r$ microdomain. Increasing the stoichiometry of PDP to 4VP stiffens the P4VP(PDP)$_r$ block. Free PDP can also be intercalated between the hydrogen-bonded PDP, further increasing the stiffness of the comb-block. This increases the entropic penalty arising from the polymer chain deformation on the incorporation of the nanoparticles. Figure 1d,e shows TEM images of a blend of PS(40)-*b*-P4VP(5.6)(PDP)$_2$ and 4 nm CdSe nanoparticles (~2 vol%). The CdSe nanoparticles formed a single layer, only one particle diameter in thickness, in the centre of the P4VP(PDP)$_2$ lamellae. TEM images were analysed to characterize the average nanoparticle position within the supramolecular assemblies (see Supplementary Fig. S6). By fitting the average nanoparticle location within the lamellae to a Gaussian function, the full-width at half-maximum is found to be 6.68 nm for the CdSe nanoparticles, 4 nm in diameter as shown in Fig. 1f. On increasing the nanoparticle loading (7 vol%, 5.4 nm PbS nanoparticles used in this case), the spatial distribution of the nanoparticles greatly narrows, relative to the size of the nanoparticle. Three-dimensional TEM tomography (see Supplementary Fig. S7) shows a stack of PbS nanoparticle sheets ~6.6 nm in thickness with a ~36 nm periodicity. Consequently, there is a strong localization of the nanoparticles to the centre of the microdomains. The deviation in the nanoparticle spatial distribution is only a fraction of the nanoparticle size,

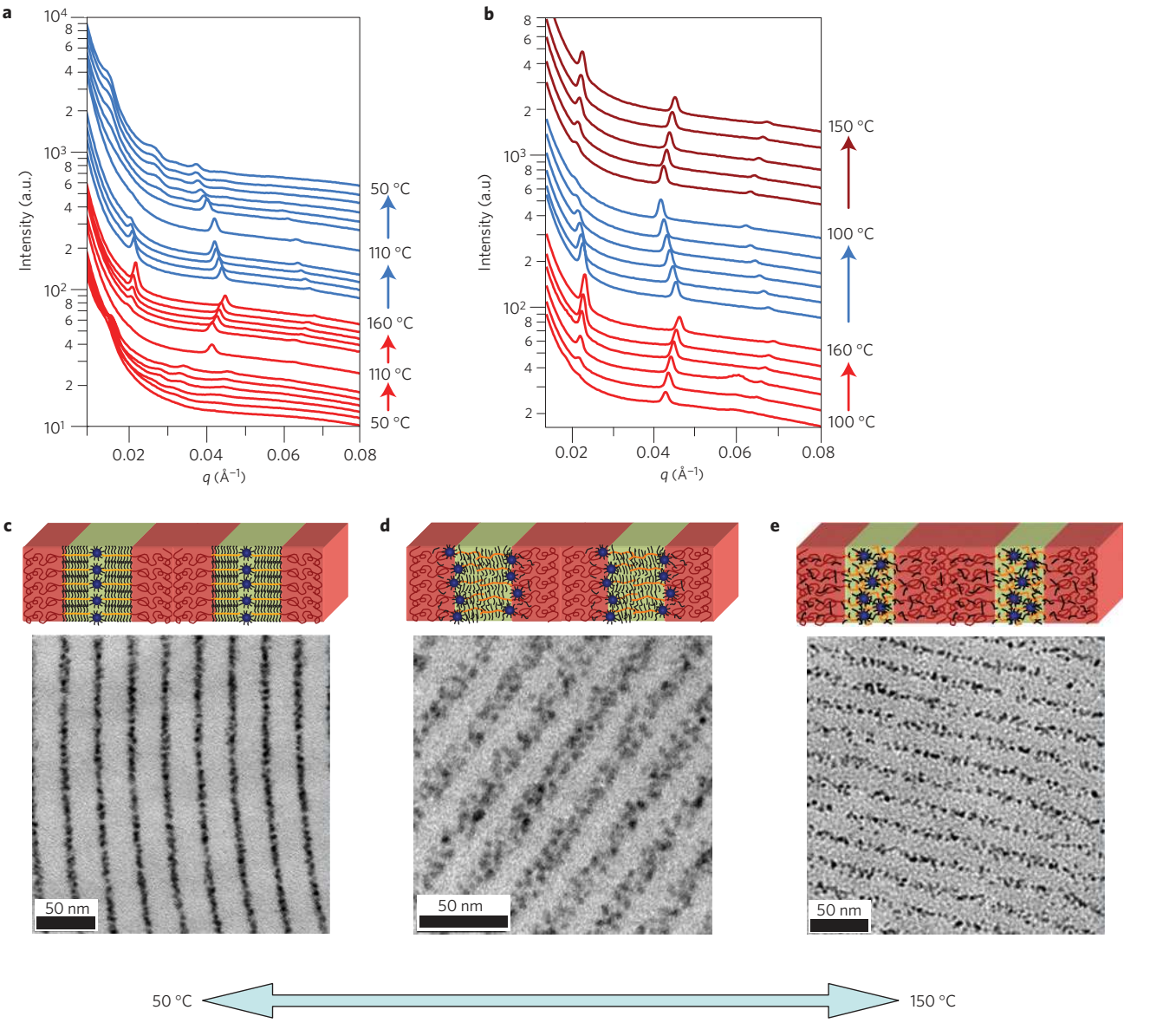

Figure 3 | *In situ* SAXS profiles of the blend of PS(40)-*b*-P4VP(5.6)(PDP)$_2$ and ~4 nm CdSe (~2 vol%) nanoparticles during the heating and cooling cycles and corresponding TEM images and schematic drawings. a, The blend was heated from 50 to 160 °C and cooled down to 50 °C at a heating/cooling rate of 10 °C min^{-1}. **b**, The blend was cycled between 100 and 160 °C. The sample was equilibrated for 10 min before SAXS images were collected. The scattering profiles were shifted vertically for clarity. Red and blue indicate the heating and cooling process, respectively. The SAXS profiles in **a** show that the blend went through two thermoreversible transitions between three assemblies of CdSe nanoparticles; that is, the nanoparticles are assembled in the centre of P4VP(PDP)$_r$ lamellae from 50 to 100 °C, at the interfaces between the polystyrene-rich and P4VP(PDP)$_r$ lamellae at 110 °C and randomly distributed in the P4VP(PDP)$_r$ lamellae at 150 °C. **c**–**e**, TEM images and schematic drawings of the blend quenched from 50 °C (**c**), 110 °C (**d**) and 150 °C (**e**). For **d**, a region with a mixture of nanoparticles assembled in the centre of lamellae and at the interfaces between lamellae was purposely selected to ensure the sample was imaged edge-on. On cycling the temperature between 100 and 160 °C, the SAXS profiles in **b** show that the peak intensity at the scattering vector range of $q = 0.02$–0.023 Å^{-1} increased during the heating cycle and decreased during the cooling cycle. This trend is exactly opposite of the peak intensity changes at the q range of 0.04–0.045 Å^{-1}. This resulted from the CdSe nanoparticles going from being localized within the lamellae, to being at the interface between two microdomains. The *in situ* SAXS profiles indicated that this thermoresponsive process is reversible.

as opposed to a few times of the size of the nanoparticles, as reported previously using BCPs alone. The precision in locating the nanoparticles spatially is comparable to that seen in the DNA approach, representing a significant improvement over existing methods. More importantly, by combining small molecules and BCPs, the nanoparticle assemblies can be readily solution-processed over arbitrarily large areas. The TEM image of a ~60 nm thin film of PS(40)-*b*-P4VP(5.6)(PDP)$_3$ and $CoFe_2O_4$ (see Supplementary Fig. S8) shows that $CoFe_2O_4$ nanoparticles assemble into chains of nanoparticles with the BCP lamellar morphology oriented normal to the surface.

Similar results were found for nanoparticles blended with supramolecules that formed cylindrical microdomains. At a PDP to P4VP ratio of 3, the volume fraction of P4VP(PDP)$_r$ increases and PS(40)-*b*-P4VP(5.6)(PDP)$_3$ forms a morphology with hexagonally packed polystyrene-rich cylinders embedded in a P4VP(PDP)$_3$ matrix (see Supplementary Fig. S9). Figure 2a,b shows TEM images of a blend of PS(40)-*b*-P4VP(5.6)(PDP)$_3$ with 5.4 nm

PbS nanoparticles (7 vol%). The TEM tomography image is shown in Fig. 2c and Supplementary Fig. S10.1. PbS nanoparticles are sequestered between the P4VP(PDP)$_r$ blocks associated with each cylindrical polystyrene microdomain and form a hexagonal grid of nanoparticles within the P4VP(PDP)$_3$ matrix. When the nanoparticle fraction is reduced, the PbS nanoparticles are preferentially sequestered to the interstitial areas of the hexagonal array forming columns of nanoparticles as shown in Fig. 2d, Supplementary Figs S10.2 and S10.3 and the schematic drawing in Fig. 2e. For PS(40)-*b*-P4VP(5.6)(PDP)$_3$ where the comb comprises the matrix, the backbone of P4VP is already stretched to form the P4VP(PDP)$_r$ comb-block. Stretching the chains further to fill the interstitial regions, which is mandated by the incompressibility of the polymer, is energetically very costly. Filling the interstitial regions with the nanoparticles reduces the required stretching and, as such, is energetically favourable. Thus, by simply adding the small molecules, the interactions between the BCP and nanoparticles and the polymer chain configuration, stiffness and packing can be readily tailored to manipulate the enthalpic and entropic contributions to the nanoparticle assembly process. Consequently, ordered arrays of nanoparticles can be assembled in one, two and three dimensions.

As the small molecules are not covalently linked to the BCP, external stimuli can be used to strengthen or weaken the bonding between the small molecules and the BCP to tailor the polymer chain configuration and architecture, as well as to alter the spatial distribution and ordering of the small molecules. Stimuli-responsive small molecules can also be readily plugged-in. This opens unique opportunities to produce responsive materials where the assembly and spatial distribution of the nanoparticles and the macroscopic properties of the nanoparticle assemblies can be altered by external stimuli. PS-*b*-P4VP(PDP)$_r$ supramolecules are thermoresponsive. The lamellae formed by the P4VP(PDP) comb-block melt at ~65 °C; the hydrogen bonding between the PDP and 4VP is stable up to 110 °C and at $T > 125$ °C, PDP is soluble in both polystyrene and P4VP and can be redistributed between the microdomains, leading to morphological transitions of the supramolecular assembly[37,38]. In the case of the supramolecule/nanoparticle blend, the thermo-responsiveness of the supramolecule can lead to a change in the dimensionality and the overall arrangements of the nanoparticle assemblies. Supplementary Fig. S11 shows an example where the redistribution of PDP changed CdSe nanoparticle assemblies from a stack of sheets into hexagonally packed cylinders.

As the small molecules can precisely tailor the enthalpic interactions and entropy in the nanoparticle assembly process, external stimuli can be used to alter both and provide greater control over the nanoparticle assembly. Figure 3a shows the *in situ* SAXS profiles of a solvent-cast blend of PS(40)-*b*-P4VP(5.6)(PDP)$_2$ with the 4 nm CdSe (2 vol%). The sample was heated from 50 to 160 °C and then cooled to 50 °C. Results for PS(40)-*b*-P4VP(5.6)(PDP)$_2$ alone are shown in Supplementary Fig. S12. The electron density difference between the nanoparticle and PS(40)-*b*-P4VP(5.6)(PDP)$_r$ is much higher than that between the polystyrene and P4VP(5.6)(PDP)$_r$ microdomains, so the SAXS profiles primarily reflect spatial distributions of the nanoparticles. After the solvent casting, the broad reflections indicate that the sample is poorly ordered and in a non-equilibrium state. On heating to 90 °C, the peak around $q = 0.0167$ Å^{-1} sharpens, corresponding to a lamellar periodicity of ~36.9 nm, as shown in the TEM image in Fig. 3c. Between 100 and 110 °C, this peak broadens and disappears with only a reflection at $q = 0.0421$ Å^{-1} evident. When the nanoparticles assemble at the interfaces, the separation distance between the nanoparticle layers was almost half that of the lamellar period, as shown in the TEM image in Fig. 3d and at 110 °C, and reflection at higher $q = 0.042$ Å^{-1} is seen.

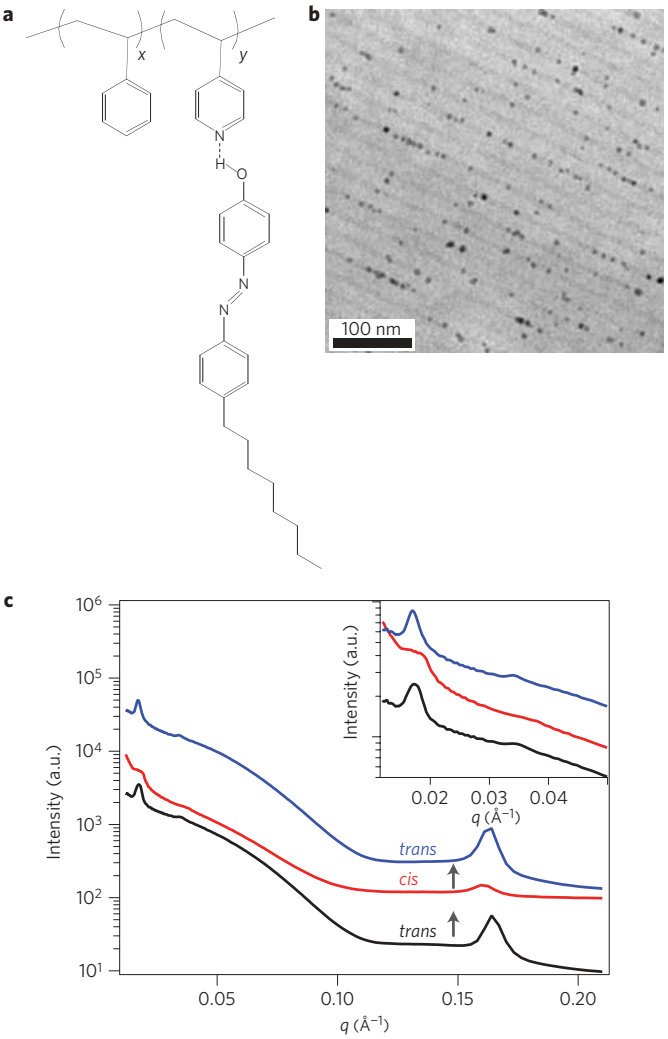

Figure 4 | Directed nanoparticle assemblies using light-responsive small molecules and BCP. a, Chemical structure of *trans*-OPAP hydrogen bonding to the 4VP in PS-*b*-P4VP. **b**, TEM image of a blend of PS(40)-*b*-P4VP(5.6)(*trans*-OPAP)$_{1.5}$ and 7 nm PbS nanoparticles (~2 vol%). **c**, SAXS profiles of a blend of PS-*b*-P4VP(OPAP)$_{1.5}$ and PbS nanoparticles (2 vol%) where the OPAPs went through isomerization from the *trans* to the *cis* and back to the *trans* state. Inset: Zoom-in view of the SAXS profiles at the low-*q* region. The *trans*–*cis* isomerization of OPAP induced a change in the periodicity of the nanoparticle assemblies from 37.4 to 32.9 nm. This is a difference of 4.5 nm or ~12% of the original lamellar spacing. With subsequent annealing under ultraviolet exposure at 419 nm, the *cis*–*trans* isomerization changed the nanoparticle assembly back.

On increasing the temperature further, a peak at $q \sim 0.0218$ Å^{-1} appears, intensifies and shifts to higher q. The CdSe nanoparticles are homogeneously distributed within the lamellar P4VP(PDP)$_r$ microdomains, as demonstrated by the TEM image in Fig. 3e and in Supplementary Fig. S14 after selective iodine staining. In the cooling cycle, a reverse process is observed. Figure 3b shows the *in situ* SAXS profiles of the same blend where the temperature was cycled between 100 and 160 °C, confirming the reversibility of the process. Thus, using temperature as a handle to direct the PDP distribution, the location of the CdSe nanoparticles was changed from the centre of the P4VP(PDP)$_r$ lamellae, to the interfaces between the lamellae and to a homogeneous dispersion in the P4VP(PDP)$_r$ lamellae. This process occurs within minutes and is fully reversible.

The *in situ* SAXS studies clearly demonstrate the power of small molecules in tailoring the thermodynamics of the nanoparticle assemblies and the versatility of the approach. The diverse nature of the nanoparticle assemblies and transitions shown reflects the delicate balance between the enthalpic and entropic contributions to the assembly nanoparticles on blending with small molecules and BCPs. The favourable interactions between the PDP and the nanoparticle ligands and its non-favourable interactions with polystyrene provide an enthalpic driving force to incorporate the nanoparticle into the P4VP(PDP)$_r$ microdomains. This is seen in the SAXS below 100 °C. As PDP solublizes in the polystyrene-rich domain, PDP mediates the polystyrene–nanoparticle interactions, reducing the driving force for selective incorporation. There is also a cross-sectional mismatch between the polystyrene coil-block and the P4VP(PDP)$_r$ comb-block that requires the polystyrene chains to be more extended at the interface, in comparison to coil–coil BCPs, which, also, increases the enthalpic contribution to the free energy. By localizing the nanoparticles at the interface between the coil- and comb-blocks, non-favourable interfacial interactions are mediated[12,42–44] and entropic penalties associated with the polystyrene chain deformation are reduced. The ramifications of these are evident in the data at 110 °C where the interfacial assembly of the nanoparticles is stabilized. Further increasing the temperature enhances the solubility of PDP in the polystyrene-rich domain. However, hydrogen bonding between PDP and 4VP is destabilized and the stiffness of the P4VP(PDP)$_r$ comb-block is decreased. Consequently, the entropic driving force for the interfacial assembly is reduced and the nanoparticles are homogeneously distributed in the P4VP(PDP)$_r$ domains at 150 °C.

The versatility of this approach lies in the non-covalent linkage between the small molecule and BCP that allows the system to respond to external stimuli, temperature in this case, and provides a simple means of controlling the local environment of the nanoparticles, the packing density of the nanoparticles and the interparticle separation distance and ordering. A wide range of supramolecules have been constructed using a variety of non-covalent linking schemes other than the hydrogen bonding used here, including electrostatic interactions or metal ligation[32,33,36]. In principle, similar types of re-organization may occur. Different small molecules with built-in responsiveness or functionality can also be substituted for PDP. A light-responsive small molecule, OPAP was attached to 4VP, forming a PS(40)-*b*-P4VP(5.6)(OPAP)$_{1.5}$ supramolecule as shown in Fig. 4a. Similar to PDP, the phenol end-group in OPAP hydrogen bonds to the 4VP unit in the BCP and the alkyl tail compatibilizes the nanoparticle's alkyl ligand. The azobenzene group responds to the light exposure and goes through a *trans–cis* isomerization when exposed to 352 nm ultraviolet light and a *cis–trans* isomerization with exposure to 419 nm radiation[45,46]. The TEM image of the PS(40)-*b*-P4VP(5.6)(OPAP)$_{1.5}$/PbS blend (~2 vol%) in Fig. 4b and the SAXS profile in Fig. 4c show that PbS nanoparticles assembled in the centre of P4VP(OPAP)$_{1.5}$ lamellae. On annealing under 352 nm ultraviolet exposure, OPAP went through a *trans–cis* isomerization and altered the periodicity of the PbS nanoparticle assembly from 37.2 to 32.9 nm, a more than 10% change in the periodicity of the nanoparticle assembly, as seen in the SAXS profiles in Fig. 4c. With subsequent annealing under 419 nm ultraviolet exposure, OPAP transformed back to the *trans* state and the nanoparticle assembly reverted to that seen in the initial PS(40)-*b*-P4VP(5.6)(OPAP)$_{1.5}$/PbS blend. Thus, the light-responsive small molecules can indeed be used to obtain responsive nanocomposite and the process was found to be fully reversible.

We have developed a very simple, yet robust approach to generate stimuli-responsive hierarchical assemblies of nanoparticles by adding small molecules to BCPs. Control over the spatial distribution of the nanoparticles over multiple length scales has been achieved. Nanocomposites responsive to heat and light are demonstrated. The use of small molecules provides an easy route to tailor the interactions between BCP and nanoparticles, direct inter-particle ordering and generate responsive interparticle ordering. The approach is versatile and applicable to a wide range of nanoparticles, opening new routes for device fabrication based on nanoparticle composite materials.

Methods

Sample preparation. Block copolymers (PS-*b*-P4VP) were purchased from Polymer Source; PDP (95%) was purchased from Acros. Chloroform was purchased from Fisher. All chemicals were used as received. A detailed description of nanoparticle synthesis can be found in Supplementary Fig. S1. PS-*b*-P4VP was first dissolved in chloroform to form 1–2% (wt/v) stock solutions. The desired amount of PDP was dissolved in chloroform. The PS-*b*-P4VP solution was then added drop-wise to the PDP solution, followed by stirring overnight. Dried nanoparticle powder was weighed and dissolved in chloroform. The PS-*b*-P4VP(PDP)$_r$ and nanoparticle solutions were mixed and stirred for one day, then cast and dried in a Teflon beaker at room temperature, allowing the solvent to slowly evaporate over 48 h. The blend was then annealed at ~100–110 °C under vacuum for 12 h and slowly cooled to room temperature.

TEM. Samples were embedded in resin (Araldite 502, Electron Microscopy Sciences) and cured at 60 °C overnight. Thin sections about 60 nm in thickness were microtomed using an RMC MT-X Ultramicrotome (Boeckler Instruments) and picked up on copper TEM grids on top of water. The thin sections were imaged using an FEI Tecnai 12 or G2 TEM at the accelerating voltages of 120 or 200 kV, respectively.

TEM tomography measurements were carried out using a JEM-2200FS (JEOL) operated at 200 kV, equipped with a slow-scan CCD (charge-coupled device) camera (Gatan USC4000, Gatan). A series of TEM images was acquired at tilt angles ranging over ±70° at an angular interval of 1°. Subsequently, the tilt series of the TEM images was aligned by the fiducial marker method using gold nanoparticles as the fiducial markers and then reconstructed on the basis of the filtered-back-projection method.

SAXS. SAXS studies were carried out at the Advanced Light Source beamline 7.3.3. X-rays with a wavelength of 1.240 Å (10 keV) were used. Spectra were collected on an ADSC Quantum 4u CCD detector with an area of 188 mm × 188 mm (2,304 pixels × 2,304 pixels). Samples for *in situ* SAXS measurements were mounted in a standard differential scanning calorimetry pan, which was used as a heating stage during scanning.

Sample preparation for Fig. 3d,e. For the samples shown in Fig. 3d,e, the samples were treated with the thermal histories described in the figure caption, using the same type of differential scanning calorimetry pan as used in the SAXS measurements. The samples were quenched by dipping into liquid nitrogen, embedded in cold-setting resin (Epofix, Electron Microscopy Sciences) and microtomed as described above. For Fig. 3d, we observed that this procedure was insufficient to trap the nanocomposite in its state at 110 °C. Both TEM and SAXS showed that a significant portion of CdSe nanoparticles returned to the centre of the P4VP(PDP) microdomain and the interfacial sequestration of the CdSe was smeared out as shown in Fig. 3d. Supplementary Fig. S13 shows a TEM image of a blend of PS-*b*-P4VP(PDP)$_2$ and ~5.4 nm PbS nanoparticles. It can be clearly seen that nanoparticles are assembled both at the centre of the lamellae and at the interfaces between the microdomains on increasing the nanoparticle volume fraction.

Received 23 June 2009; accepted 1 October 2009; published online 18 October 2009

References

1. Aldaye, F. A., Palmer, A. L. & Sleiman, H. F. Assembling materials with DNA as the guide. *Science* **321,** 1795–1799 (2008).
2. Balazs, A. C., Emrick, T. & Russell, T. P. Nanoparticle polymer composites: Where two small worlds meet. *Science* **314,** 1107–1110 (2006).
3. Boal, A. K. *et al.* Self-assembly of nanoparticles into structured spherical and network aggregates. *Nature* **404,** 746–748 (2000).
4. Glotzer, S. & Solomon, M. Anisotropy of building blocks and their assembly into complex structures. *Nature Mater.* **6,** 557–562 (2007).
5. Huynh, W. U., Dittmer, J. J. & Alivisatos, A. P. Hybrid nanorod-polymer solar cells. *Science* **295,** 2425–2427 (2002).
6. Li, Q. F. *et al.* Responsive assemblies: Gold nanoparticles with mixed ligands in microphase separated block copolymers. *Adv. Mater.* **20,** 1462–1466 (2008).
7. Costanzo, P. J. & Beyer, F. L. Thermally driven assembly of nanoparticles in polymer matrices. *Macromolecules* **40,** 3996–4001 (2007).
8. Alivisatos, A. P. *et al.* Organization of 'nanocrystal molecules' using DNA. *Nature* **382,** 609–611 (1996).

9. Mirkin, C. A., Letsinger, R. L., Mucic, R. C. & Storhoff, J. J. A DNA-based method for rationally assembling nanoparticles into macroscopic materials. *Nature* **382,** 607–609 (1996).
10. Bockstaller, M. R., Mickiewicz, R. A. & Thomas, E. L. Block copolymer nanocomposites: Perspectives for tailored functional materials. *Adv. Mater.* **17,** 1331–1349 (2005).
11. Chiu, J. J., Kim, B. J., Kramer, E. J. & Pine, D. J. Control of nanoparticle location in block copolymers. *J. Am. Chem. Soc.* **127,** 5036–5037 (2005).
12. Lin, Y. *et al.* Self-directed self-assembly of nanoparticle/copolymer mixtures. *Nature* **434,** 55–59 (2005).
13. Mackay, M. E. *et al.* General strategies for nanoparticle dispersion. *Science* **311,** 1740–1743 (2006).
14. Shenhar, R., Norsten, T. B. & Rotello, V. M. Polymer-mediated nanoparticle assembly: Structural control and applications. *Adv. Mater.* **17,** 657–669 (2005).
15. Lopes, W. A. & Jaeger, H. M. Hierarchical self-assembly of metal nanostructures on diblock copolymer scaffolds. *Nature* **414,** 735–738 (2001).
16. Thompson, R. B., Ginzburg, V. V., Matsen, M. W. & Balazs, A. C. Predicting the mesophases of copolymer-nanoparticle composites. *Science* **292,** 2469–2472 (2001).
17. Bockstaller, M. R., Lapetnikov, Y., Margel, S. & Thomas, E. L. Size-selective organization of enthalpic compatibilized nanocrystals in ternary block copolymer/particle mixtures. *J. Am. Chem. Soc.* **125,** 5276–5277 (2003).
18. Lauter-Pasyuk, V. *et al.* Effect of nanoparticle size on the internal structure of copolymer-nanoparticles composite thin films studied by neutron reflection. *Physica B* **241,** 1092–1094 (1997).
19. Lee, J. Y., Thompson, R. B., Jasnow, D. & Balazs, A. C. Entropically driven formation of hierarchically ordered nanocomposites. *Phys. Rev. Lett.* **89,** 155503 (2002).
20. Spontak, R. *et al.* Selectivity- and size-induced segregation of molecular and nanoscale species in microphase-ordered triblock copolymers. *Nano Lett.* **6,** 2115–2120 (2006).
21. Matsen, M. W. & Thompson, R. B. Particle distributions in a block copolymer nanocomposite. *Macromolecules* **41,** 1853–1860 (2008).
22. Glogowski, E., Tangirala, R., Russell, T. P. & Emrick, T. Functionalization of nanoparticles for dispersion in polymers and assembly in fluids. *J. Polym. Sci. Polym. Chem.* **44,** 5076–5086 (2006).
23. Kim, B. J., Fredrickson, G. H. & Kramer, E. J. Effect of polymer ligand molecular weight on polymer-coated nanoparticle location in block copolymers. *Macromolecules* **41,** 436–447 (2008).
24. Chiu, J. J. *et al.* Distribution of nanoparticles in lamellar domains of block copolymers. *Macromolecules* **40,** 3361–3365 (2007).
25. Tsutsumi, K., Funaki, Y., Hirokawa, Y. & Hashimoto, T. Selective incorporation of palladium nanoparticles into microphase-separated domains of poly(2-vinylpyridine)-block-polyisoprene. *Langmuir* **15,** 5200–5203 (1999).
26. Huh, J., Ginzburg, V. V. & Balazs, A. C. Thermodynamic behavior of particle/diblock copolymer mixtures: Simulation and theory. *Macromolecules* **33,** 8085–8096 (2000).
27. Templeton, A. C., Wuelfing, M. P. & Murray, R. W. Monolayer protected cluster molecules. *Acc. Chem. Res.* **33,** 27–36 (2000).
28. Hong, R., Fischer, N. O., Emrick, T. & Rotello, V. M. Surface pegylation and ligand exchange chemistry of FePt nanoparticles for biological applications. *Chem. Mater.* **17,** 4617–4621 (2005).
29. Owen, J. S., Park, J., Trudeau, P. & Alivisatos, A. P. Reaction chemistry and ligand exchange at cadmium-selenide nanocrystal surfaces. *J. Am. Chem. Soc.* **130,** 12279–12281 (2008).
30. Beard, M. C. *et al.* Variations in the quantum efficiency of multiple exciton generation for a series of chemically treated PbSe nanocrystal films. *Nano Lett.* **9,** 836–845 (2009).
31. Kato, T. & Fréchet, J. M. J. Stabilization of a liquid-crystalline phase through noncovalent interaction with a polymer side-chain. *Macromolecules* **22,** 3818–3819 (1989).
32. Antonietti, M., Conrad, J. & Thunemann, A. Polyelectrolyte-surfactant complexes—a new-type of solid, mesomorphous material. *Macromolecules* **27,** 6007–6011 (1994).
33. Ruokolainen, J. *et al.* Poly(4-vinyl pyridine)/zinc dodecyl benzene sulfonate mesomorphic state due to coordination complexation. *Macromolecules* **28,** 7779–7784 (1995).
34. Ober, C. K. & Wegner, G. Polyelectrolyte-surfactant complexes in the solid state: Facile building blocks for self-organizing materials. *Adv. Mater.* **9,** 17–31 (1997).
35. Stewart, D. & Imrie, C. T. Toward supramolecular side-chain liquid crystal polymers. 5. The template receptor approach. *Macromolecules* **30,** 877–884 (1997).
36. Ikkala, O. & ten Brinke, G. Hierarchical self-assembly in polymeric complexes: Towards functional materials. *Chem. Commun.* 2131–2137 (2004).
37. Ruokolainen, J. *et al.* Switching supramolecular polymeric materials with multiple length scales. *Science* **280,** 557–560 (1998).
38. Valkama, S. *et al.* Self-assembled structures in diblock copolymers with hydrogen-bonded amphiphilic plasticizing compounds. *Macromolecules* **39,** 9327–9336 (2006).
39. White, T. J., Serak, S. V., Tabiryan, N. V., Vaia, R. A. & Bunning, T. J. Polarization-controlled, photodriven bending in monodomain liquid crystal elastomer cantilevers. *J. Mater. Chem.* **19,** 1080–1085 (2009).
40. Saariaho, M., Subbotin, A., Szleifer, I., Ikkala, O. & ten Brinke, G. Effect of side chain rigidity on the elasticity of comb copolymer cylindrical brushes: A monte carlo simulation study. *Macromolecules* **32,** 4439–4443 (1999).
41. Ruokolainen, J. *et al.* Supramolecular routes to hierarchical structures: Comb–coil diblock copolymers organized with two length scales. *Macromolecules* **32,** 1152–1158 (1999).
42. Lin, Y., Skaff, H., Emrick, T., Dinsmore, A. D. & Russell, T. P. Nanoparticle assembly and transport at liquid–liquid interfaces. *Science* **299,** 226–229 (2003).
43. Kim, B. J. *et al.* Creating surfactant nanoparticles for block copolymer composites through surface chemistry. *Langmuir* **23,** 12693–12703 (2007).
44. Kim, B. J., Fredrickson, G. H., Hawker, C. J. & Kramer, E. J. Nanoparticle surfactants as a route to bicontinuous block copolymer morphologies. *Langmuir* **23,** 7804–7809 (2007).
45. Brode, W. R., Gould, J. H. & Wyman, G. M. Phototropism and cis–trans isomerism in aromatic azo compounds. *J. Am. Chem. Soc.* **74,** 4641–4646 (1952).
46. Eisenbach, C. D. Effect of polymer matrix on cis–trans isomerization of azobenzene residues in bulk polymers. *Makromol. Chem.* **179,** 2489–2506 (1978).

Acknowledgements

We thank T. P. Russell for the valuable discussions. SAXS experiments were carried out at beamline 7.3.3 at the Advanced Light Source. $CoFe_2O_4$ nanoparticle was provided by the Molecular Foundry at Lawrence Berkeley National Laboratory. This was supported by the Army Research Office STIR program under award No. W911NF-07-1-0653; NSF DMR-0805301; by the DuPont Young Professor Grant and by the 3 M Nontenured Faculty Grant. This work was also supported by the Director, Office of Science, Office of Basic Energy Sciences, of the US Department of Energy under Contract No. DE-AC02-05CH11231 through the 'Organic-inorganic Nanocomposites' programme at LBNL. H.J. acknowledges support from the Ministry of Education, Science, Sports and Culture through Grants-in-Aid No. 19031016, 21015017, 21106512 and 21241030.

Author contributions

T.X. conceived and guided the project. Y.Z., K.T. and A.J.M. carried out sample preparation, measurements and data analyses detailed in the article. T.S. carried out the initial exploration and B.J.R. carried out the experiments using light responsive molecules. K.M. and H.J. carried out TEM tomography on select samples. J.M.L., Y.W. and A.P.A. provided the nanoparticles used. D.P. and J.M.J.F. synthesized the OPAP.

Additional information

Supplementary information accompanies this paper on www.nature.com/naturematerials. Reprints and permissions information is available online at http://npg.nature.com/reprintsandpermissions. Correspondence and requests for materials should be addressed to T.X.